Journal of
Marine Science and Engineering

MDPI

Article

Undrained Triaxial Shear Tests on Hydrate-Bearing Fine-Grained Sediments from the Shenhu Area of South China Sea

Ruchun Wei [1,2,3,4], Lele Liu [2,3,*], Chao Jia [1,4,*], Xiao Dong [1,4], Qingtao Bu [2,3], Yongchao Zhang [2,3], Changling Liu [2,3] and Nengyou Wu [2,3]

[1] Institute of Marine Science and Technology, Shandong University, Qingdao 266232, China
[2] Laboratory for Marine Mineral Resources, Qingdao National Laboratory for Marine Science and Technology, Qingdao 266237, China
[3] Key Laboratory of Gas Hydrate, Ministry of Natural Resources, Qingdao Institute of Marine Geology, Qingdao 266237, China
[4] The Key Laboratory of Geological Safety of Coastal Urban Underground Space, Ministry of Natural Resources, Shandong University, Qingdao 266232, China
* Correspondence: lele.liu@qnlm.ac (L.L.); jiachao@sdu.edu.cn (C.J.)

Abstract: Changes in undrained shear strength are important to the stability analysis of hydrate reservoirs during natural gas hydrate production. This study proposes a prediction model of undrained shear strength of hydrate-bearing fine-grained sediments based on the critical state theory. Several consolidated undrained triaxial shear tests are conducted on hydrate-bearing fine-grained samples from the Shenhu area of the South China Sea. The effects of effective consolidation stresses and hydrate saturations on the undrained shear strength are investigated. The results show that the undrained shear strength increases linearly with increasing effective consolidation stress. When the hydrate saturation is greater than the effective hydrate saturation, the undrained shear strength significantly increases with increasing hydrate saturation. The undrained shear strength of hydrate-bearing fine-grained sediments is a two-parameter function of effective hydrate saturation and a void ratio. The instability risk of the hydrate reservoir under undrained conditions is greater than that of under-drained or partially drained conditions. Furthermore, low-porosity reservoirs face more shear strength loss from hydrate decomposition yet lower risk than high-porosity ones. These results can improve the understanding of mechanical properties of hydrate-bearing fine-grained sediments under undrained conditions. This study also has implications for the design of marine structures in areas with hydrate-bearing sediment.

Keywords: natural gas hydrate; fine-grained sediment; critical state theory; effective hydrate saturation; stability analysis

Citation: Wei, R.; Liu, L.; Jia, C.; Dong, X.; Bu, Q.; Zhang, Y.; Liu, C.; Wu, N. Undrained Triaxial Shear Tests on Hydrate-Bearing Fine-Grained Sediments from the Shenhu Area of South China Sea. *J. Mar. Sci. Eng.* **2023**, *11*, 1604. https://doi.org/10.3390/jmse11081604

Academic Editor: Timothy S. Collett

Received: 18 July 2023
Revised: 7 August 2023
Accepted: 9 August 2023
Published: 16 August 2023

1. Introduction

Natural gas hydrates (NGHs) have been treated as a potential energy resource for decades because of their vast reserve and wide distribution in nature [1–3]. In recent years, several countries have carried out a series of production tests in the field to evaluate the possibility of different methods for the commercial production of NGHs [4–8]. The results clearly indicate that depressurization is a method with the highest production efficiency and the maximum probability of being commercialized [9–14]. The application effect of depressurization to marine NGHs is largely controlled by the hydraulic permeability of hydrate-bearing sediments which is highly stress dependent [15–19]. The stress of hydrate-bearing sediments generally increases during depressurization, and mechanical properties of hydrate-bearing sediments weaken due to NGHs dissociation [20–22]. In addition, NGHs dissociation can also be driven by climatic, oceanic, and geologic processes [23–27], and ultimately has a great potential to cause shear failures and trigger various geohazards [28–31]. In particular, for hydrate deposits in the Shenhu area of the

South China Sea [32,33], the fine-grained hydrate-bearing sediments are of low hydraulic permeabilities, and this implies that pore water and gas produced by NGHs dissociation due to underlying warm oil extraction and global warming can hardly flow out of pores in a short period, corresponding to an undrained condition [15,34–36]. Undrained shear properties of hydrate-bearing fine-grained sediments are of great significance to the stability of marine sediments and overburden structures.

Mechanical properties (e.g., shear strength, stiffness, and dilatancy) of hydrate-bearing sediments are largely dependent on hydrate saturation (i.e., a ratio of hydrate volume to the total pore volume) and hydrate pore habits [37–39]. With regard to mechanical properties, the hydrate pore habits mainly include pore-filling, load-bearing, and grain-cementing [40]. Debonding and/or crushing of NGHs within pores of coarse-grained sediments will occur during shearing [41]. However, the failure mechanism of hydrate-bearing fine-grained sediments has not been well understood since whether the cementation between clay and silt particles by NGHs exists or not remains elusive [42,43]. There is no doubt that NGHs behave as a solid filler of host sediments to reduce the effective void ratio (i.e., a ratio of fluid-occupied pore volume to the solid volume) of hydrate-bearing sediments [44–46], and the alteration of the effective void ratio affects the undrained shear strength of hydrate-bearing fine-grained sediments. For example, Yoneda et al. [47] found that there is a linear relationship between the undrained shear strength and the void ratio of fine-grained natural cores. Yun et al. [48] reported that the undrained shear strength of saturated natural cores acquired from the Gulf of Mexico is a function of water saturation. The enhancement effect to the effective void ratio due to NGHs dissociation is coupled with a reduction effect by compression deformation because of the increasing effective stress during depressurization. This makes it very challenging to predict the undrained shear strength of hydrate-bearing fine-grained sediments. Several prediction models have been proposed based on the Mohr-Coulomb criterion [49,50], and the models can give acceptable results in certain circumstances.

Critical state soil mechanics provides a theoretical framework to predict the undrained shear strength of saturated hydrate-free sediments with different void ratios [51]. The enhanced undrained shear strength of hydrate-bearing sediments can be captured by using an extended yield surface [52]. The extended yield surface in p'–q space is shown as a thick line in Figure 1, and the extension is an explicit product of multiple effects caused by the presence of NGHs. For details, Effect I represents that hydrate-free sediments can reach point A under an effective mean normal stress p'_0, indicating the yield surface of hydrate-free sediments shown as a thin solid line. The extension expressed as Effect II in the figure represents the observed strength enhancement due to the presence of NGHs within pores of marine sediments [53]. Since NGHs within pores have the potential to hinder volumetric deformation during consolidation [54], the void ratio of host sediments is generally larger than that of hydrate-free sediments when the effective mean normal stress is the same. This indicates that the yield surface of host sediments shown as a thin dashed line in Figure 1 is smaller than that of hydrate-free sediments, corresponding to the weakening effect (i.e., Effect III) of NGHs on the host sediments [55]. From this point of view, the intrinsic strength enhancement due to the presence of NGHs expressed as Effect IV in the figure is larger than the observed strength enhancement. For prediction model developments for mechanical properties (e.g., the undrained shear strength) of hydrate-bearing sediments, the intrinsic void ratio and shear strength enhancements due to the presence of NGHs within pores should be jointly considered.

To investigate the effects of effective consolidation stresses and hydrate saturations on the undrained shear strength on hydrate-bearing fine-grained sediments, this study performs undrained triaxial shear tests, and the experimental results are further used to validate a prediction model proposed based on the critical state theory in this study. The host sediments for hydrate formation are remodeled by using natural sediments acquired from the Shenhu area of the South China Sea, and the joint effect of hydrate is considered in the prediction model. This study has great potential to facilitate geotechnical designs of marine and submarine structures overlying hydrate-bearing sediments in nature.

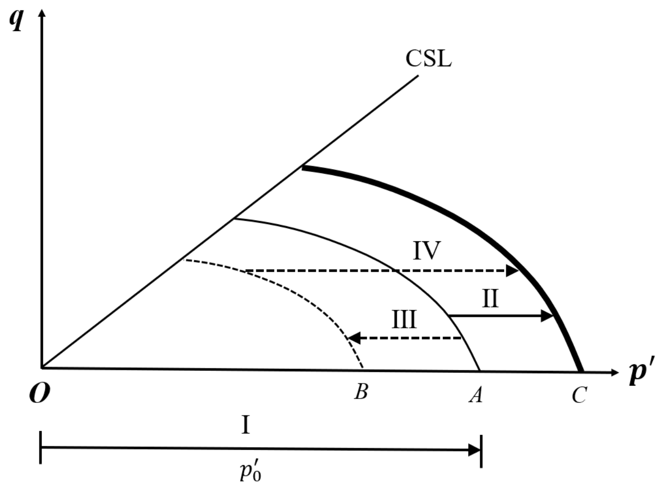

Figure 1. Yield surfaces in p'–q space for hydrate-free (the thin solid line) and hydrate-bearing (the thick solid line) sediments. The symbol p' stands for the effective mean normal stress, and q for the generalized shear stress. The abbreviation CSL represents the critical state line of soils.

2. Experimental Program

2.1. Experimental Apparatus and Materials

The experimental apparatus used in this study for undrained triaxial shear tests on hydrate-bearing sediments is upgraded from a commercialized triaxial shear test system manufactured by the Jiangsu Yongchang Science and Education Instrument Limited Company. A high-pressure test cell, resisting inner pressure up to 25 MPa, is applied instead of classic clear acrylic chambers, and an air bath is added to lower the temperature for hydrate formation. The load frame for triaxial shearing has a capacity of 250 kN, and the strain rate can be well controlled at a selected value ranging from 0.001 mm/min to 3 mm/min. A linear variable differential transformer (LVDT) produced by the Shanghai Tianmu Company is applied to measure the axial displacement, and the comprehensive accuracy is 0.1% of full scale (F.S). The axial force during triaxial shearing is measured by using a stress sensor with a comprehensive accuracy of 0.2% F.S. For more details about the apparatus, please refer to Dong et al. [56].

Clayey and silty sediments acquired from the Shenhu area in South China Sea are used to remodel host sediments for hydrate formation in this study. The grain size ranges from ~1 μm to 200 μm, and the median grain size is 13.9 μm. For more information about physical properties of marine sediments, please refer to Wei et al. [57]. Since methane hydrate formation within pores of fine-grained sediments is technically difficult and extremely time-consuming, tetrahydrofuran (THF) is selected as an analog of methane gas to form hydrate with pore water. Previous studies have shown that physical and mechanical properties of hydrate-bearing sediments are mostly dependent on hydrate occurrence characteristics [38,39,58]. The pore habit of THF hydrate is generally consistent with that of NGHs in nature [59]. Therefore, this analog is widely adopted in the gas hydrate community for experimental studies on mechanical properties of hydrate-bearing fine-grained sediments [60–62].

2.2. Procedure for Host Sediment Preparation

The procedure for host sediment preparation in this study is briefly summarized as follows: (i) The natural sediments are air-dried and then well mixed with some THF solution to acquire an initial solution content of 15% by weight; (ii) the moist sediments are sealed in a bag to distribute the solution for 12 h; (iii) the moist sediments are remodeled to form a cylindrical specimen with a diameter of 38 mm and a height of 76 mm as host sediments for hydrate formation; (iv) the vacuum method is applied to fully saturate the host sediments, and the saturation time is longer than 24 h. THF solutions with different mass ratios of THF and water are used to control hydrate saturation, and a void ratio of the host sediments is selected according to the porosity logging data.

2.3. Procedure for Hydrate Formation and Triaxial Shearing

In this study, consolidation is conducted before hydrate formation to avoid the hindering effect of pore hydrate on compression deformation. During the consolidation, the pore pressure is kept at the atmospheric pressure, and the confining pressure is enhanced by a rate of 100 kPa/min until a selected effective confining pressure is reached. The whole period of consolidation is generally longer than 24 h. After full consolidation, saturated host sediments are cooled, and the temperature is controlled at around 0 °C for 4 days to form THF hydrate. Then, the temperature is adjusted to 3 °C higher and kept for 2 days to eliminate potential ice within pores of hydrate-bearing sediments. For hydrate-free sediments, the consolidation and freezing procedures are also applied, but using pure water instead of a THF solution. Undrained triaxial shearing with a constant rate of 0.04%/min is performed on hydrate-bearing sediments, and the shearing is stopped when the axial strain reaches 15%. According to ASTM D2216 [63], the water content determined after triaxial shearing can be used to calculate the effective and intrinsic void ratios of hydrate-bearing sediments.

2.4. Test Design

To simulate the real case in the Shenhu area of the South China Sea [64,65], values of the initial porosity of host sediments are controlled as 0.525, 0.500, and 0.482, corresponding to the initial void ratios of 1.105, 1.000, and 0.932. To avoid over-consolidation, values of the effective confining pressure are set as 1.0 MPa, 2.0 MPa, and 3.0 MPa based on the void ratio vs. the consolidation stress curve [57]. Values of hydrate saturation are selected as 0%, 30%, and 50%, corresponding to the THF vs. water mass ratios of 0, 0.060, and 0.104 [15].

3. Results

3.1. Effects of Effective Consolidation Stress on the Undrained Shear Strength

Stress–strain curves under different conditions of the effective consolidation stress (i.e., confining pressure) are shown in Figure 2. It is obvious that all the curves are strain hardening, in which the generalized shear stress q (i.e., the deviatoric stress for triaxial shear tests) constantly increases with increasing axial strain ε_a. Values of the peak deviatoric stress q_f (i.e., two times the undrained shear strength S_u) under different conditions are summarized in Table 1, and the q_f-value increases with increasing effective consolidation stress. Values of the intrinsic void ratio e after triaxial shearing are also listed in Table 1. It is generally accepted that e-value decreases with increasing effective consolidation stress, leading to higher q_f-value of hydrate-bearing sediments. Figure 3 shows how the undrained shear strength of hydrate-free and hydrate-bearing sediments evolves with effective consolidation stress (i.e., confining pressure) and hydrate saturation. It is obvious that the undrained shear strength S_u linearly increases with increasing effective consolidation stress p'_0, and the fitted slope is 0.57, 0.78, and 1.67 for S_h = 0%, 30%, and 50%, respectively.

Table 1. Key information of undrained triaxial shear tests on hydrate-free and hydrate-bearing sediments in this study. (Note e_0 for the intrinsic void ratio of host sediments before consolidation, p'_0 for the effective consolidation stress, S_h for the hydrate saturation, q_f for the peak strength in stress–strain curves, and e for the intrinsic void ratio of sediments after triaxial shearing.).

e_0	p'_0 (MPa)	S_h (%)	q_f (MPa)	e
1.105	1	0	1.16	1.063
		30	1.86	1.120
		50	7.64	1.051

Table 1. *Cont.*

e_0	p'_0 (MPa)	S_h (%)	q_f (MPa)	e
		0	2.32	0.993
1	2	30	3.72	0.898
		50	11.30	0.924
		0	3.42	0.917
0.932	3	30	4.98	0.854
		50	14.32	0.890

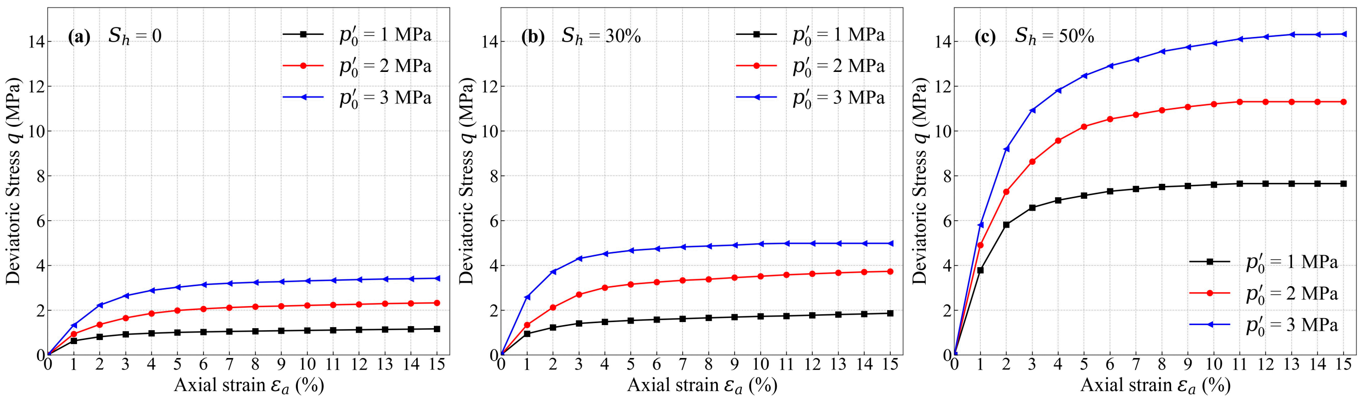

Figure 2. Stress–strain curves of hydrate-free (**a**) and hydrate-bearing sediments under different effective consolidation stresses (i.e., confining pressures) p'_0. The hydrate saturations S_h are 30% (**b**) and 50% (**c**).

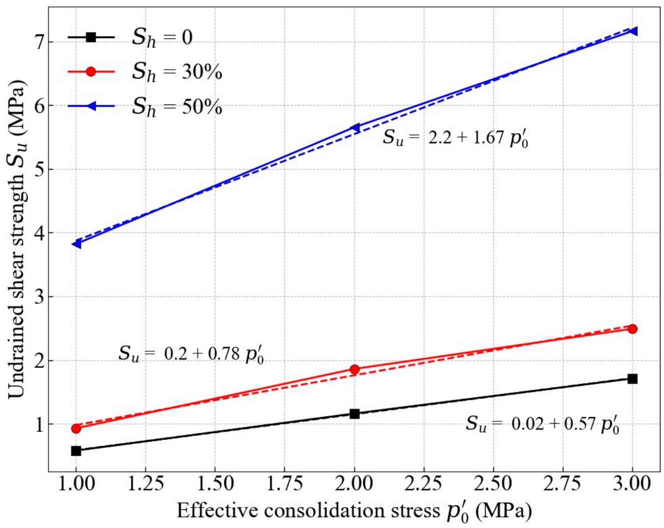

Figure 3. The undrained shear strength S_u of hydrate-free and hydrate-bearing sediments under different effective consolidation stresses p'_0.

3.2. Effects of Hydrate Saturation on the Undrained Shear Strength

Figure 4 shows the stress–strain curves of marine sediments with different hydrate saturations S_h. It is obvious that the q_f value increases with increasing S_h when the effective consolidation stress p'_0 is the same. For example, q_f = 2.32 MPa for S_h = 0% when p'_0 = 2.0 MPa, q_f = 3.72 MPa for S_h = 30%, and q_f = 11.3 MPa for S_h = 50%. The increasing hydrate saturation S_h reduces the effective void ratio of hydrate-bearing sediments, leading to increasing q_f. This is consistent with the results of Yang et al. [20]. In addition, the stress–strain curves for hydrate saturation equaling 50% are significantly higher than those for lower hydrate saturations. This indicates that the increasing hydrate saturation S_h

has a stronger effect on the elevating q_f of hydrate-bearing sediments than the increasing effective consolidation stress p'_0. Figure 5 shows the undrained shear strength S_u under different hydrate saturations S_h. It is clearly shown that the increase is nonlinear, and the increment of S_u for S_h increasing from 0% to 30% is significantly smaller than that for S_h increasing from 30% to 50%. This implies that there is a critical hydrate saturation S_{he} beyond which the undrained shear strength enhancement becomes much more obvious. The critical hydrate saturation is lower than 30%, and this is consistent with the results of De La Fuente et al. [66].

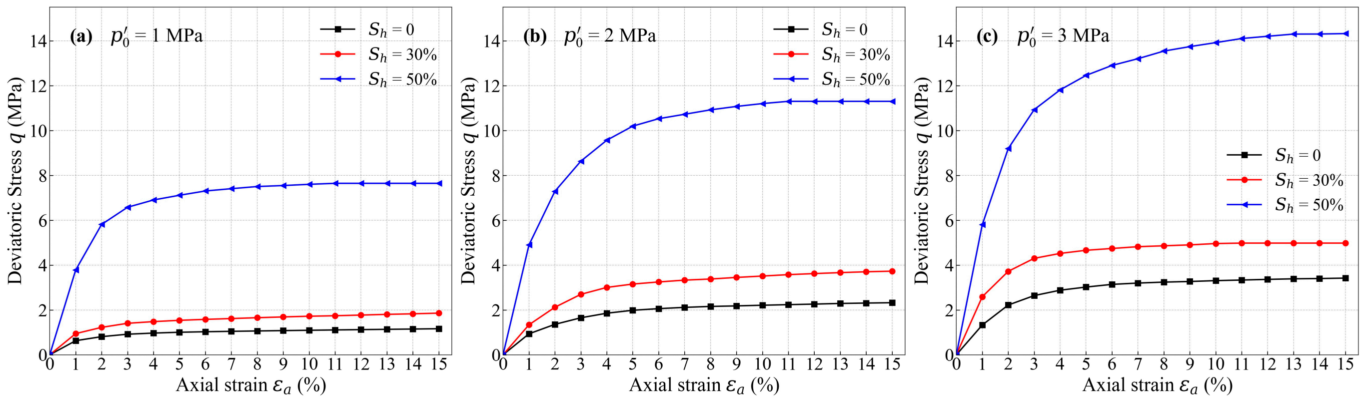

Figure 4. Stress–strain curves of marine sediments with different hydrate saturations S_h. p'_0 = 1.0 MPa (**a**), 2.0 MPa (**b**), and 3.0 MPa (**c**).

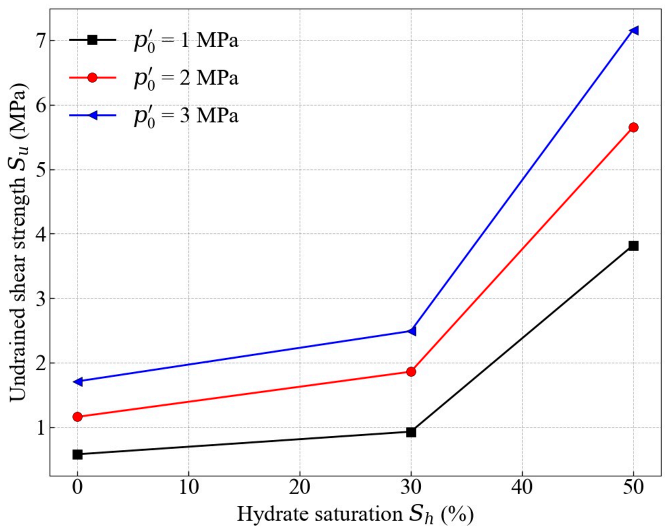

Figure 5. The undrained shear strength S_u of hydrate-free and hydrate-bearing sediments with different hydrate saturations S_h.

4. Development and Validation of a Theoretical Model for Predicting the Undrained Shear Strength

4.1. Development of the Prediction Model

According to critical state soil mechanics [51], the undrained shear strength S_u of saturated hydrate-free sediments can be predicted by:

$$S_u = \frac{M}{2} \exp\left(\frac{\Gamma - \nu}{\lambda}\right) \tag{1}$$

where M is stress ratio at the critical state; Γ is the specific volume intercept of the critical state line, and λ is the slope of the critical state line; ν represents specific volume and equals to 1 + e. In addition, M, Γ, λ, and ν are dimensionless parameters.

Equation (1) represents that the undrained shear strength of saturated hydrate-free sediments depends on the void ratio regardless of the consolidation history. For saturated hydrate-bearing sediments, solid hydrate occupies the pore space and reduces the effective specific volume. However, not all the pore hydrate has obvious effects on mechanical properties of hydrate-bearing sediments, and an effective hydrate saturation S_{he} is adopted. Yan et al. [67] propose a simple equation to determine S_{he} as follows:

$$S_{he} = \langle S_h - \xi S_{hc} \rangle \tag{2}$$

where $\langle\ \rangle$ is the Macaulay bracket. When value of $S_h - \xi S_{hc}$ is larger than zero, the value of S_{he} is equal to that of $S_h - \xi S_{hc}$, while the value of S_{he} is equal to zero when the value of $S_h - \xi S_{hc}$ is lower than zero. Values of critical hydrate saturation S_{hc} are within a range from 25% to 40% [43], and S_{hc} = 25% in this study. Parameter ξ represents different effects of different hydrate pore habits, and ξ = 0 for cementing the hydrate while ξ = 1 for non-cementing (e.g., pore-filling and load-bearing) hydrate.

By treating pore hydrate as part of the solid skeleton, the effective void ratio of hydrate-bearing sediments e_h is calculated as $e \cdot (1 - S_{he})/(1 + e \cdot S_{he})$. Therefore, the effective specific volume ν_h of hydrate-bearing sediments is expressed as:

$$\nu_h = \frac{1+e}{1+e \cdot S_{he}} \tag{3}$$

Combining Equations (1)–(3), a prediction model for the undrained shear strength of hydrate-bearing fine-grained sediments is proposed as:

$$\begin{cases} S_{hu} = \frac{M}{2}\exp\left(\frac{\Gamma-\nu_h}{\lambda}\right) = \frac{M}{2}\exp\left(\frac{\Gamma-\frac{1+e}{1+e\cdot S_{he}}}{\lambda}\right) \\ S_{he} = \langle S_h - \xi S_{hc} \rangle \end{cases} \tag{4}$$

Based on the critical state soil mechanics, when sediments reach the critical state, all the properties of structure within the sediments would be destroyed [51]. Therefore, parameters M, Γ, and λ are constant corresponding to the host sediments regardless of hydrate saturation [68,69]. Values of ξ and S_{hc} are related to hydrate pore habits [70]. Since it is difficult to form fully cementing hydrate within fine-grained sediments [43], ξ is equal to 1 in this study. Values of hydrate saturation S_h and effective void ratio e are measured during triaxial shear tests.

4.2. Validation of the Prediction Model

A series of consolidated undrained shear tests on hydrate-free sediments have been performed [57], and the results are used to fit for parameter value extraction (Figure 6). It is obvious that M = 1.28, Γ = 3.25, and λ = 0.175. These values are applied in this study, and the predicted results for hydrate-bearing sediments are shown in Figure 7. It is clearly shown that the predicted values are well consistent with measured values when the hydrate saturation is no larger than 30%. However, the predicted results are significantly higher than the test results for the specimen with a hydrate saturation of 50%. There are two possible reasons for this discrepancy: (i) the specimen with S_h = 50% has a relatively high density, and shear failure may occur before specimens reach the critical state; (ii) possible error in the critical hydrate saturation S_{hc} will lead to uncertainties in the calculated results of the effective hydrate saturation S_{he}.

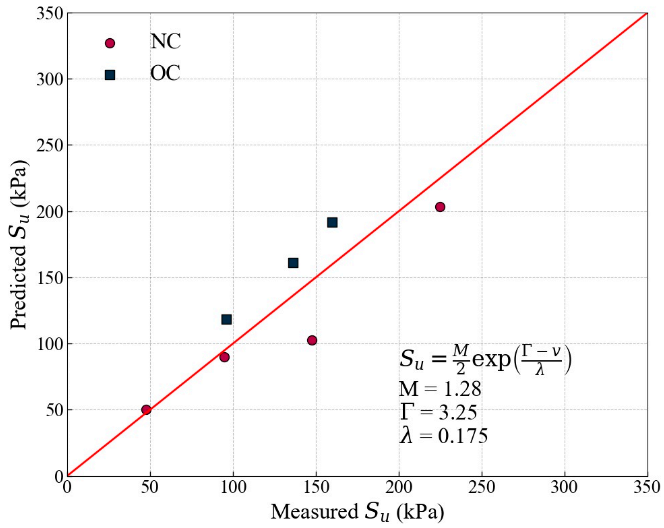

Figure 6. Predicted and measured values of the undrained shear strength S_u of hydrate-free sediments. The abbreviation NC stands for normal consolidated, and OC for over-consolidated. The measured values are from Wei et al. [57]. The model used in this figure is Equation (1).

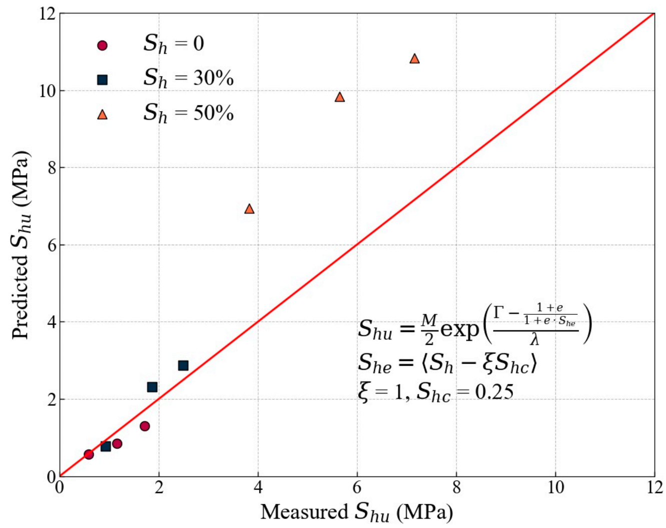

Figure 7. Predicted and measured values of the undrained shear strength S_{hu} of hydrate-bearing sediments in this study. The model used in this figure is Equation (4).

To further explain the effect of S_{hc} on the accuracy of the prediction model, values of the undrained shear strength with different critical hydrate saturations are calculated by using the prediction model, and the variation curves are shown in Figure 8. Mean void ratios of 1.078, 0.933, and 0.887 corresponding to p_0' = 1.0 MPa, 2.0 MPa, and 3 MPa are used for calculation, and the arrows represent the overall increasing trend of S_{hc}. It is shown that the undrained shear strength decreases with increasing critical hydrate saturation. The test results with a hydrate saturation of 30% are on the curve with S_{hc} = 0.25, while the test results with a hydrate saturation of 50% are near the curve with S_{hc} = 0.30. Therefore, it can be inferred that the difference in prediction accuracy depends on the value of critical hydrate saturation S_{hc}. The results also indicate that mechanical properties of hydrate-bearing sediments are dependent on hydrate pore habits. For pore-filling hydrate, its effect only occurs when hydrate saturation S_h exceeds its effective hydrate saturation S_{he} [66]. The magnitude of effective hydrate saturation S_{he} is controlled by the critical hydrate saturation S_{hc} according to the proposed model in this study. Therefore, the value of critical hydrate saturation is crucial for the accuracy of model prediction results. Based on the comparison between the experimental data and theoretical calculation results shown in Figure 8, an empirical model is proposed to correct the effective hydrate saturation S_{he}:

$$S_{he} = \langle S_h - \xi(S_h + a) \cdot S_{hc} \rangle \tag{5}$$

where a is an empirical parameter, and a = 0.7 in this study.

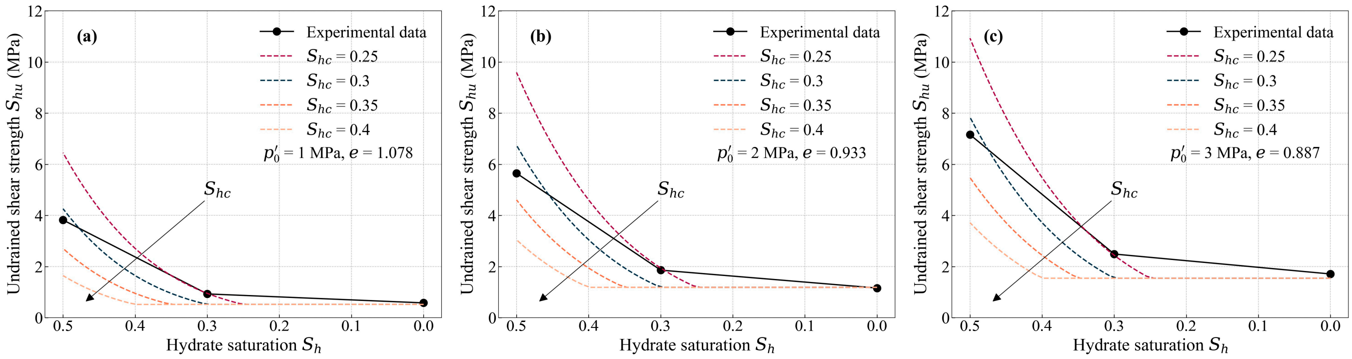

Figure 8. Effects of the critical hydrate saturation S_{hc} on the undrained shear strength of hydrate-bearing sediments S_{hu} under different consolidation stresses p'_0 = 1.0 MPa (**a**), 2.0 MPa (**b**), and 3.0 MPa (**c**). Colored dashed lines are drawn by using the prediction model of Equation (4).

Thus, the modified prediction model is expressed as:

$$\begin{cases} S_{hu} = \frac{M}{2} \exp\left(\frac{\Gamma - \frac{1+e}{1+e \cdot S_{he}}}{\lambda}\right) \\ S_{he} = \langle S_h - (S_h + a) S_{hc} \rangle \end{cases} \tag{6}$$

The prediction results calculated by using the modified prediction model are compared with the experimental data (Figure 9). It is shown that the corrected prediction results agree well with the experimental results. It is concluded that the undrained shear strength of hydrate-bearing fine-grained sediments is jointly affected by the effective hydrate saturation S_{he} and the effective void ratio e. The accuracy of the effective hydrate saturation S_{he} is dependent on value of the critical hydrate saturation S_{hc}.

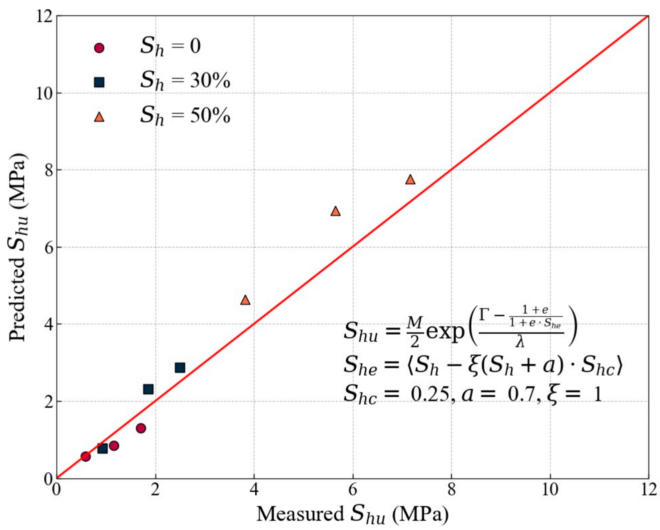

Figure 9. Predicted and measured values of the undrained shear strength of hydrate-bearing sediments S_{hu} in this study. The model used in this figure is Equation (6).

5. Implications to the Production of NGHs in Nature

Values of S_u with different hydrate saturations and porosities are calculated by using the modified prediction model, and the variation curves are shown in Figure 10. It is shown that hydrate dissociation obviously leads to a reduction in the undrained shear strength of hydrate-bearing sediments. However, if consolidation of the sediments is allowed, the increasing undrained shear strength due to the reduction in porosity would compensate for the loss in the undrained shear strength caused by hydrate decomposition. For sediments with an initial hydrate saturation of 0.5 and an initial porosity of 0.525, if the hydrate is completely decomposed and undergoes consolidated deformation with a final porosity of 0.425. The undrained shear strength before and after hydrate decomposition is almost the same. However, the equilibrium of undrained shear strength variation is not achieved for all conditions. For example, for sediments with an initial porosity of 0.475, and all other conditions being unchanged, the undrained shear strength would not exceed the initial state even if the consolidation is completed. Although the stability of the reservoirs benefits from the decrease in porosity, it will in turn greatly reduce the permeability limiting the extraction efficiency [71]. Therefore, further research is needed to explore the balance of stability and efficiency.

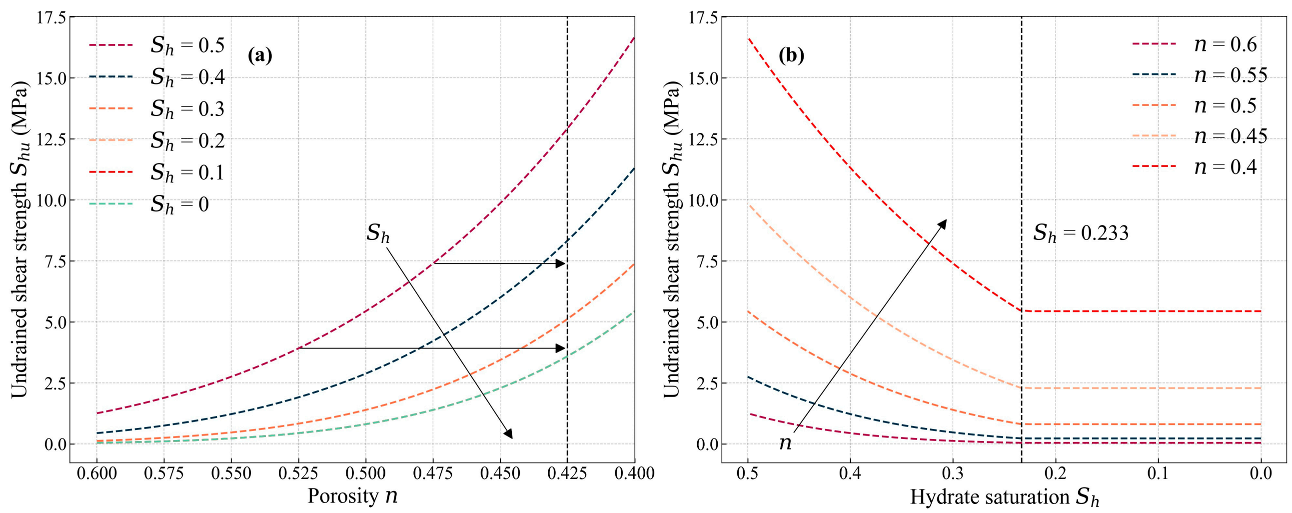

Figure 10. Calculated values of the undrained shear strength of hydrate-bearing sediments S_{hu} under different conditions of hydrate saturation (**a**) and porosity (**b**). Colored dashed lines are acquired by using Equation (6).

Under the condition that the porosity remains constant with hydrate saturation decreasing, the lower the porosity, the more obvious the effect of hydrate decomposition on its undrained shear strength (Figure 10b). Furthermore, the continued decrease in hydrate saturation does not cause a further decrease in the undrained shear strength when the hydrate saturation is lower than 0.233. The hydrate decomposition leads to a decrease in the density of sediments and thus its undrained shear strength. There is a lower limit of the undrained shear strength. This lower limit is related to the intrinsic porosity of host sediments. The magnitude of the lower limit of sediments with low porosity is greater than that of sediments with high porosity. Therefore, although the loss of undrained shear strength of reservoirs with low porosity is greater than that of reservoirs with high porosity during hydrate decomposition, the former has a lower instability risk than the latter.

To summarize, the results are of great potential to the stability analysis of hydrate reservoirs in marine and cold environments, and the design of structures for production [72,73]. The instability risk of the hydrate reservoir under undrained conditions is greater than that of under-drained or partially drained conditions. This is because there is a strength compensation caused by consolidated deformation although hydrate decomposition causes a decrease in the shear strength of reservoirs. For example, hydrate reservoirs in the South

China Sea are mainly composed of fine-grained sediments [33,74]. Since the fine-grained sediments are of low hydraulic permeabilities, the excess pore pressure caused by changes in stress states tends to be accumulated within the reservoirs during NGH production. This, in turn, leads to decreasing effective stress which promotes the possibility of submarine slope instability.

6. Conclusions

A prediction model of undrained shear strength of hydrate-bearing fine-grained sediments is developed based on the critical state theory. Several consolidated undrained triaxial shear tests are conducted on remodeled specimens. The effects of effective consolidation stresses and hydrate saturations on the undrained shear strength are investigated. The prediction model is validated using the test results, and reasonably corrected. The main conclusions are as follows:

(1) Values of q_f increase with increasing effective consolidation stress and hydrate saturation. There is a linear relationship between undrained shear strength and effective consolidation stress, while when the hydrate saturation is greater than the effective hydrate saturation, the undrained shear strength significantly increases with increasing hydrate saturation.
(2) The undrained shear strength of hydrate-bearing fine-grained sediments is a two-parameter function of effective hydrate saturation and void ratio.
(3) The instability risk of the hydrate reservoir under undrained conditions is greater than that of under-drained or partially drained conditions. This is because of that although hydrate decomposition causes a decrease in the shear strength of reservoirs, there is a strength compensation caused by consolidated deformation.
(4) The decrease in the undrained shear strength caused by the hydrate decomposition has a lower limit. This lower limit is related to the own porosity of host sediments. Low porosity reservoirs face more shear strength loss from hydrate decomposition yet lower risk than high porosity ones.

Admittedly, there are uncertainties in the effect of hydrate occurrences on parameters ξ and S_{hc}. Especially, since all the hydrate-bearing specimens undergo consolidation before hydrate generation in the test procedure, the effect of consolidation stress on hydrate occurrences is not considered. In addition, the validation of hydrate saturations ranged from 0 to 0.5. The higher hydrate saturation is needed to be further verified. Therefore, it is necessary to carry out more consolidated undrained triaxial shear tests on hydrate-bearing fine-grained sediments to improve the prediction model.

Author Contributions: Conceptualization, R.W., L.L. and C.J.; methodology, R.W.; validation, R.W. and X.D.; formal analysis, L.L.; investigation, Y.Z.; resources, C.L.; data curation, X.D.; writing—original draft preparation, R.W.; writing—review and editing, L.L. and C.J.; visualization, R.W. and X.D.; supervision, Q.B., Y.Z. and C.L.; funding acquisition, L.L., Q.B. and N.W. All authors have read and agreed to the published version of the manuscript.

Funding: This study is jointly supported by the National Natural Science Foundation of Shandong Province (grant number ZR2022YQ54), the Open Research Fund Program of State key Laboratory of Hydroscience and Engineering (grant number sklhse-2022-D-03), the Marine S&T Fund of Shandong Province for Pilot National Laboratory for Marine Science and Technology (Qingdao) (grant number 2021QNLM020002), the Taishan Scholars Program (grant number tsqn202306297), and the China Geological Survey (Project DD20230064).

Institutional Review Board Statement: Not applicable.

Informed Consent Statement: Not applicable.

Data Availability Statement: All data have been provided in the paper.

Conflicts of Interest: The authors declare no conflict of interest.

Abbreviations

CSL	critical state line
CU	consolidated undrained
e	void ratio
v	specific volume, equals to 1 + e
v_h	specific volume of hydrate-bearing sediments
M	stress ratio at the critical state
NC	normally consolidated
NGHs	natural gas hydrates
OC	over consolidated
p'_0	effective confining pressure
p'	mean effective stress, equal to $(\sigma'_1 + 2\sigma'_3)/3$
q	deviatoric stress, equal to $\sigma_1 - \sigma_3$
q_f	deviatoric stress at failure
SCS	South China Sea
S_h	hydrate saturation
S_{hc}	critical hydrate saturation
S_{he}	effective hydrate saturation
S_u	undrained shear strength, equal to $q_f/2$
S_{hu}	undrained shear strength of hydrate-bearing sediments
w	water content
ε_a	axial strain
Γ	specific volume intercept of the critical state line
λ	slope of the critical state line

References

1. Kvenvolden, K.A. Gas hydrates-geological perspective and global change. *Rev. Geophys.* **1993**, *31*, 173–187. [CrossRef]
2. Sloan, E.D. Fundamental principles and applications of natural gas hydrates. *Nature* **2003**, *426*, 353–359. [CrossRef] [PubMed]
3. Collett, T.; Bahk, J.-J.; Baker, R.; Boswell, R.; Divins, D.; Frye, M.; Goldberg, D.; Husebø, J.; Koh, C.; Malone, M.; et al. Methane Hydrates in Nature—Current Knowledge and Challenges. *J. Chem. Eng. Data* **2015**, *60*, 319–329. [CrossRef]
4. Wang, Z.; Zhang, Y.; Peng, Z.; Shan, Z.; Sun, B.; Sun, J. Recent Advances in Methods of Gas Recovery from Hydrate-Bearing Sediments: A Review. *Energy Fuels* **2022**, *36*, 5550–5593. [CrossRef]
5. Kurihara, M.; Sato, A.; Funatsu, K.; Ouchi, H.; Yamamoto, K.; Numasawa, M.; Ebinuma, T.; Narita, H.; Masuda, Y.; Dallimore, S.R.; et al. Analysis of Production Data for 2007/2008 Mallik Gas Hydrate Production Tests in Canada. In *Proceedings of the All Days*; SPE-132155-MS; SPE: Richardson, TX, USA, 2010.
6. Rossi, F.; Gambelli, A.M. Thermodynamic phase equilibrium of single-guest hydrate and formation data of hydrate in presence of chemical additives: A review. *Fluid Phase Equilibria* **2021**, *536*, 112958. [CrossRef]
7. Mahmood, M.N.; Guo, B. Gas production from marine gas hydrate reservoirs using geothermal-assisted depressurization method. *Adv. Geo-Energy Res.* **2023**, *7*, 90–98. [CrossRef]
8. Liu, L.; Lu, X.; Zhang, X.; Liu, C.; Du, B. Numerical simulations for analyzing deformation characteristics of hydrate-bearing sediments during depressurization. *Adv. Geo-Energy Res.* **2017**, *1*, 135–147. [CrossRef]
9. Ye, J.; Qin, X.; Xie, W.; Lu, H.; Ma, B.; Qiu, H.; Liang, J.; Lu, J.; Kuang, Z.; Lu, C.; et al. The second natural gas hydrate production test in the South China Sea. *China Geol.* **2020**, *3*, 197–209. [CrossRef]
10. Li, J.; Ye, J.; Qin, X.; Qiu, H.; Wu, N.; Lu, H.; Xie, W.; Lu, J.; Peng, F.; Xu, Z.; et al. The first offshore natural gas hydrate production test in South China Sea. *China Geol.* **2018**, *1*, 5–16. [CrossRef]
11. Yamamoto, K.; Terao, Y.; Fujii, T.; Ikawa, T.; Seki, M.; Matsuzawa, M.; Kanno, T. Operational overview of the first offshore production test of methane hydrates in the Eastern Nankai Trough. In Proceedings of the Offshore Technology Conference, Houston, TX, USA, 5–8 May 2014; pp. 1–15.
12. Anderson, B.; Hancock, S.; Wilson, S.; Enger, C.; Collett, T.; Boswell, R.; Hunter, R. Formation pressure testing at the Mount Elbert Gas Hydrate Stratigraphic Test Well, Alaska North Slope: Operational summary, history matching, and interpretations. *Mar. Pet. Geol.* **2011**, *28*, 478–492. [CrossRef]
13. Boswell, R.; Schoderbek, D.; Collett, T.S.; Ohtsuki, S.; White, M.; Anderson, B.J. The Iġnik Sikumi Field Experiment, Alaska North Slope: Design, Operations, and Implications for CO_2–CH_4 Exchange in Gas Hydrate Reservoirs. *Energy Fuels* **2017**, *31*, 140–153. [CrossRef]
14. Yamamoto, K.; Wang, X.-X.; Tamaki, M.; Suzuki, K. The second offshore production of methane hydrate in the Nankai Trough and gas production behavior from a heterogeneous methane hydrate reservoir. *RSC Adv.* **2019**, *9*, 25987–26013. [CrossRef] [PubMed]
15. Zhang, Z.; Liu, L.; Ning, F.; Liu, Z.; Sun, J.; Li, X.; Sun, J.; Hyodo, M.; Liu, C. Effect of stress on permeability of clay silty cores recovered from the Shenhu hydrate area of the South China Sea. *J. Nat. Gas Sci. Eng.* **2022**, *99*, 104421. [CrossRef]

16. Huang, L.; Su, Z.; Wu, N.; Cheng, J. Analysis on geologic conditions affecting the performance of gas production from hydrate deposits. *Mar. Pet. Geol.* **2016**, *77*, 19–29. [CrossRef]
17. Okwananke, A.; Hassanpouryouzband, A.; Vasheghani Farahani, M.; Yang, J.; Tohidi, B.; Chuvilin, E.; Istomin, V.; Bukhanov, B. Methane recovery from gas hydrate-bearing sediments: An experimental study on the gas permeation characteristics under varying pressure. *J. Pet. Sci. Eng.* **2019**, *180*, 435–444. [CrossRef]
18. Dai, S.; Kim, J.; Xu, Y.; Waite, W.F.; Jang, J.; Yoneda, J.; Collett, T.S.; Kumar, P. Permeability anisotropy and relative permeability in sediments from the National Gas Hydrate Program Expedition 02, offshore India. *Mar. Pet. Geol.* **2019**, *108*, 705–713. [CrossRef]
19. Santamarina, J.C.; Dai, S.; Terzariol, M.; Jang, J.; Waite, W.F.; Winters, W.J.; Nagao, J.; Yoneda, J.; Konno, Y.; Fujii, T.; et al. Hydro-bio-geomechanical properties of hydrate-bearing sediments from Nankai Trough. *Mar. Pet. Geol.* **2015**, *66*, 434–450. [CrossRef]
20. Yang, D.; Yan, R.; Yan, M.; Lu, D.; Wei, C. Geomechanical properties of artificial methane hydrate-bearing fine-grained sediments. *Gas Sci. Eng.* **2023**, *109*, 104852. [CrossRef]
21. Konno, Y.; Fujii, T.; Sato, A.; Akamine, K.; Naiki, M.; Masuda, Y.; Yamamoto, K.; Nagao, J. Key Findings of the World's First Offshore Methane Hydrate Production Test off the Coast of Japan: Toward Future Commercial Production. *Energy Fuels* **2017**, *31*, 2607–2616. [CrossRef]
22. Kato, A.; Konno, Y.; Yoneda, J.; Kida, M.; Oshima, M.; Jin, Y.; Nagao, J.; Tenma, N. Evaluation of failure modes and undrained shear strength by cone penetrometer for Natural Gas hydrate-bearing pressure-core sediment samples recovered from the Krishna–Godavari Basin, offshore India. *Mar. Pet. Geol.* **2019**, *108*, 502–511. [CrossRef]
23. Biastoch, A.; Treude, T.; Rüpke, L.H.; Riebesell, U.; Roth, C.; Burwicz, E.B.; Park, W.; Latif, M.; Böning, C.W.; Madec, G.; et al. Rising Arctic Ocean temperatures cause gas hydrate destabilization and ocean acidification. *Geophys. Res. Lett.* **2011**, *38*, L08602. [CrossRef]
24. Phrampus, B.J.; Hornbach, M.J. Recent changes to the Gulf Stream causing widespread gas hydrate destabilization. *Nature* **2012**, *490*, 527–530. [CrossRef] [PubMed]
25. Wallmann, K.; Riedel, M.; Hong, W.L.; Patton, H.; Hubbard, A.; Pape, T.; Hsu, C.W.; Schmidt, C.; Johnson, J.E.; Torres, M.E.; et al. Gas hydrate dissociation off Svalbard induced by isostatic rebound rather than global warming. *Nat. Commun.* **2018**, *9*, 83. [CrossRef]
26. Burton, Z.F.M.; Kroeger, K.F.; Hosford Scheirer, A.; Seol, Y.; Burgreen-Chan, B.; Graham, S.A. Tectonic Uplift Destabilizes Subsea Gas Hydrate: A Model Example From Hikurangi Margin, New Zealand. *Geophys. Res. Lett.* **2020**, *47*, e2020GL087150. [CrossRef]
27. Burton, Z.F.M.; Dafov, L.N. Salt Diapir-Driven Recycling of Gas Hydrate. *Geochem. Geophys. Geosyst.* **2023**, *24*, e2022GC010704. [CrossRef]
28. Sultan, N.; Cochonat, P.; Foucher, J.-P.; Mienert, J. Effect of gas hydrates melting on seafloor slope instability. *Mar. Geol.* **2004**, *213*, 379–401. [CrossRef]
29. Dhakal, S.; Gupta, I. Slope instability of submarine sediments due to hydrate dissociation: A case study of Northern Cascadia Margin. *Geoenergy Sci. Eng.* **2023**, *223*, 211558. [CrossRef]
30. Maslin, M.; Owen, M.; Betts, R.; Day, S.; Dunkley Jones, T.; Ridgwell, A. Gas hydrates: Past and future geohazard? *Philos. Trans. R. Soc. A Math. Phys. Eng. Sci.* **2010**, *368*, 2369–2393. [CrossRef]
31. Sun, Y.; Lu, H.; Lu, C.; Li, S.; Lv, X. Hydrate dissociation induced by gas diffusion from pore water to drilling fluid in a cold wellbore. *Adv. Geo-Energy Res.* **2018**, *2*, 410–417. [CrossRef]
32. Bai, C.; Su, P.; Su, X.; Cui, H.; Shang, W.; Han, S.; Zhang, G. Characterization of the sediments in a gas hydrate reservoir in the northern South China Sea: Implications for gas hydrate accumulation. *Mar. Geol.* **2022**, *453*, 106912. [CrossRef]
33. Ning, F.; Liang, J.; Wu, N.; Zhu, Y.; Wu, S.; Liu, C.; Wei, C.; Wang, D.; Zhang, Z.; Xu, M.; et al. Reservoir characteristics of natural gas hydrates in China. *Nat. Gas Ind.* **2020**, *40*, 1–24. [CrossRef]
34. Wei, R.; Jia, C.; Liu, L.; Wu, N. Analysis of the Characteristics of Pore Pressure Coefficient for Two Different Hydrate-Bearing Sediments under Triaxial Shear. *J. Mar. Sci. Eng.* **2022**, *10*, 509. [CrossRef]
35. Wei, J.; Yang, L.; Liang, Q.; Liang, J.; Lu, J.; Zhang, W.; Zhang, X.; Lu, X. Geomechanical properties of gas hydrate-bearing sediments in Shenhu Area of the South China Sea. *Energy Rep.* **2021**, *7*, 8013–8020. [CrossRef]
36. Priest, J.A.; Hayley, J.L.; Smith, W.E.; Schultheiss, P.; Roberts, J. PCATS triaxial testing: Geomechanical properties of sediments from pressure cores recovered from the Bay of Bengal during expedition NGHP-02. *Mar. Pet. Geol.* **2019**, *108*, 424–438. [CrossRef]
37. Wu, Y.; Liao, J.; Zhang, W.; Cui, J. Characterization of stress–dilatancy behavior for methane hydrate-bearing sediments. *J. Nat. Gas Sci. Eng.* **2021**, *92*, 104000. [CrossRef]
38. Hyodo, M.; Li, Y.; Yoneda, J.; Nakata, Y.; Yoshimoto, N.; Nishimura, A.; Song, Y. Mechanical behavior of gas-saturated methane hydrate-bearing sediments. *J. Geophys. Res. Solid Earth* **2013**, *118*, 5185–5194. [CrossRef]
39. Hassanpouryouzband, A.; Joonaki, E.; Vasheghani Farahani, M.; Takeya, S.; Ruppel, C.; Yang, J.; English, N.J.; Schicks, J.M.; Edlmann, K.; Mehrabian, H.; et al. Gas hydrates in sustainable chemistry. *Chem. Soc. Rev.* **2020**, *49*, 5225–5309. [CrossRef]
40. Wu, P.; Li, Y.; Sun, X.; Liu, W.; Song, Y. Mechanical Characteristics of Hydrate-Bearing Sediment: A Review. *Energy Fuels* **2021**, *35*, 1041–1057. [CrossRef]
41. Pinkert, S.; Grozic, J.L.H. Failure Mechanisms in Cemented Hydrate-Bearing Sands. *J. Chem. Eng. Data* **2015**, *60*, 376–382. [CrossRef]

42. Wu, P.; Li, Y.; Wang, L.; Sun, X.; Wu, D.; He, Y.; Li, Q.; Song, Y. Hydrate-bearing sediment of the South China Sea: Microstructure and mechanical characteristics. *Eng. Geol.* **2022**, *307*, 106782. [CrossRef]
43. Waite, W.F.; Santamarina, J.C.; Cortes, D.D.; Dugan, B.; Espinoza, D.N.; Germaine, J.; Jang, J.; Jung, J.W.; Kneafsey, T.J.; Shin, H.; et al. Physical properties of hydrate-bearing sediments. *Rev. Geophys.* **2009**, *47*, RG4003. [CrossRef]
44. Zhan, L.; Liu, B.; Zhang, Y.; Lu, H. Rock Physics Modeling of Acoustic Properties in Gas Hydrate-Bearing Sediment. *J. Mar. Sci. Eng.* **2022**, *10*, 1076. [CrossRef]
45. Guo, Z.; Lv, X.; Liu, C.; Chen, H.; Cai, Z. Characterizing Gas Hydrate–Bearing Marine Sediments Using Elastic Properties—Part 1: Rock Physical Modeling and Inversion from Well Logs. *J. Mar. Sci. Eng.* **2022**, *10*, 1379. [CrossRef]
46. Guo, Z.; Lv, X.; Liu, C.; Chen, H.; Mei, L. Characterizing Gas Hydrate-Bearing Marine Sediments Using Elastic Properties—Part 2: Seismic Inversion Based on a Pore-Filling–Solid Matrix Decoupling Scheme. *J. Mar. Sci. Eng.* **2022**, *10*, 1497. [CrossRef]
47. Yoneda, J.; Masui, A.; Konno, Y.; Jin, Y.; Egawa, K.; Kida, M.; Ito, T.; Nagao, J.; Tenma, N. Mechanical properties of hydrate-bearing turbidite reservoir in the first gas production test site of the Eastern Nankai Trough. *Mar. Pet. Geol.* **2015**, *66*, 471–486. [CrossRef]
48. Yun, T.S.; Narsilio, G.A.; Carlos Santamarina, J. Physical characterization of core samples recovered from Gulf of Mexico. *Mar. Pet. Geol.* **2006**, *23*, 893–900. [CrossRef]
49. Yan, R.; Yu, H.; Yang, D.; Tang, H.; Zhang, Q. Shear strength and pore pressure characteristics of methane hydrate-bearing soil under undrained condition. *Int. J. Hydrogen Energy* **2023**, *48*, 12240–12256. [CrossRef]
50. Liu, W.; Chen, P.; Wu, P.; You, Z.; Wang, L.; Huang, L.; Zhang, S.; Yu, T.; Li, Y. Mechanical Characteristics of Underconsolidated Methane Hydrate-Bearing Clayed-Silty Sediments. *Energy Fuels* **2023**, *37*, 6503–6514. [CrossRef]
51. Wood, D.M. *Soil Behaviour and Critical State Soil Mechanics*; Cambridge University Press: Cambridge, UK, 1991; ISBN 9780521332491.
52. Uchida, S.; Soga, K.; Yamamoto, K. Critical state soil constitutive model for methane hydrate soil. *J. Geophys. Res. Solid Earth* **2012**, *117*. [CrossRef]
53. Kong, L.; Wang, X.; Hua, L.; Lin, X. A bounding surface model of gas-hydrate-bearing sediments. *Environ. Geotech.* **2023**, *10*, 196–205. [CrossRef]
54. Yoneda, J.; Oshima, M.; Kida, M.; Kato, A.; Konno, Y.; Jin, Y.; Tenma, N. Consolidation and hardening behavior of hydrate-bearing pressure-core sediments recovered from the Krishna–Godavari Basin, offshore India. *Mar. Pet. Geol.* **2019**, *108*, 512–523. [CrossRef]
55. Zhou, J.; Yang, Z.; Wei, C.; Chen, P.; Yan, R. Mechanical behavior of hydrate-bearing sands with fine particles under isotropic and triaxial compression. *J. Nat. Gas Sci. Eng.* **2021**, *92*, 103991. [CrossRef]
56. Dong, L.; Li, Y.; Liao, H.; Liu, C.; Chen, Q.; Hu, G.; Liu, L.; Meng, Q. Strength estimation for hydrate-bearing sediments based on triaxial shearing tests. *J. Pet. Sci. Eng.* **2020**, *184*, 106478. [CrossRef]
57. Wei, R.; Liu, L.; Jia, C.; Zhao, H.; Dong, X.; Bu, Q.; Liu, C.; Wu, N. Undrained Shear Properties of Shallow Clayey-Silty Sediments in the Shenhu Area of South China Sea. *Sustainability* **2023**, *15*, 1175. [CrossRef]
58. Lee, J.Y.; Yun, T.S.; Santamarina, J.C.; Ruppel, C. Observations related to tetrahydrofuran and methane hydrates for laboratory studies of hydrate-bearing sediments. *Geochem. Geophys. Geosyst.* **2007**, *8*. [CrossRef]
59. Liu, Z.; Kim, J.; Lei, L.; Ning, F.; Dai, S. Tetrahydrofuran Hydrate in Clayey Sediments—Laboratory Formation, Morphology, and Wave Characterization. *J. Geophys. Res. Solid Earth* **2019**, *124*, 3307–3319. [CrossRef]
60. Yun, T.S.; Santamarina, J.C.; Ruppel, C. Mechanical properties of sand, silt, and clay containing tetrahydrofuran hydrate. *J. Geophys. Res. Solid Earth* **2007**, *112*. [CrossRef]
61. Kim, J.; Seol, Y.; Dai, S. The coefficient of earth pressure at rest in hydrate-bearing sediments. *Acta Geotech.* **2021**, *16*, 2729–2739. [CrossRef]
62. Liu, Z.; Dai, S.; Ning, F.; Peng, L.; Wei, H.; Wei, C. Strength Estimation for Hydrate-Bearing Sediments From Direct Shear Tests of Hydrate-Bearing Sand and Silt. *Geophys. Res. Lett.* **2018**, *45*, 715–723. [CrossRef]
63. *Stand. ASTM D2216-19*; ASTM Standard Test Method for Laboratory Determination of Water (Moisture) Content of Soil and Rock by Mass. ASTM: West Conshohocken, PA, USA, 2019.
64. Wang, X.; Hutchinson, D.R.; Wu, S.; Yang, S.; Guo, Y. Elevated gas hydrate saturation within silt and silty clay sediments in the Shenhu area, South China Sea. *J. Geophys. Res.* **2011**, *116*, B05102. [CrossRef]
65. Kuang, Y.; Yang, L.; Li, Q.; Lv, X.; Li, Y.; Yu, B.; Leng, S.; Song, Y.; Zhao, J. Physical characteristic analysis of unconsolidated sediments containing gas hydrate recovered from the Shenhu Area of the South China sea. *J. Pet. Sci. Eng.* **2019**, *181*, 106173. [CrossRef]
66. De La Fuente, M.; Vaunat, J.; Marín-Moreno, H. Consolidation of gas hydrate-bearing sediments with hydrate dissociation. *E3S Web Conf.* **2020**, *205*, 11007. [CrossRef]
67. Yan, R.T.; Liang, W.Y.; Wei, C.F.; Wu, E.L. A constitutive model for gas hydrate-bearing sediments considering hydrate occurring habits. *Yantu Lixue/Rock Soil Mech.* **2017**, *38*, 10–18. [CrossRef]
68. Sultan, N.; Garziglia, S. Geomechanical constitutive modelling of gas-hydrate-bearing sediments. In Proceedings of the 7th International Conference on Gas Hydrates, Edinburgh, UK, 17–21 July 2011; pp. 1–11.
69. Fang, H.; Shi, K.; Yu, Y. A state-dependent subloading constitutive model with unified hardening function for gas hydrate-bearing sediments. *Int. J. Hydrogen Energy* **2022**, *47*, 4441–4471. [CrossRef]
70. Yan, R.; Wei, C. Constitutive Model for Gas Hydrate–Bearing Soils Considering Hydrate Occurrence Habits. *Int. J. Géoméch.* **2017**, *17*, 4017032. [CrossRef]

71. Zhao, Y.; Liu, J.; Sang, S.; Hua, L.; Kong, L.; Zeng, Z.; Yuan, Q. Experimental investigation on the permeability characteristics of methane hydrate-bearing clayey-silty sediments considering various factors. *Energy* **2023**, *269*, 126811. [CrossRef]
72. Vasheghani Farahani, M.; Hassanpouryouzband, A.; Yang, J.; Tohidi, B. Insights into the climate-driven evolution of gas hydrate-bearing permafrost sediments: Implications for prediction of environmental impacts and security of energy in cold regions. *RSC Adv.* **2021**, *11*, 14334–14346. [CrossRef]
73. Fetisov, V.; Ilyushin, Y.V.; Vasiliev, G.G.; Leonovich, I.A.; Müller, J.; Riazi, M.; Mohammadi, A.H. Development of the automated temperature control system of the main gas pipeline. *Sci. Rep.* **2023**, *13*, 3092. [CrossRef]
74. Li, J.; Lu, J.; Kang, D.; Ning, F.; Lu, H.; Kuang, Z.; Wang, D.; Liu, C.; Hu, G.; Wang, J.; et al. Lithological characteristics and hydrocarbon gas sources of gas hydrate-bearing sediments in the Shenhu area, South China Sea: Implications from the W01B and W02B sites. *Mar. Geol.* **2019**, *408*, 36–47. [CrossRef]